# Cardiac Unfold: A Novel Technique for Image-Guided Cardiac Catheterization Procedures

YingLiang Ma[1], Rashed Karim[1], R. James Housden[1], Geert Gijsbers[2], Roland Bullens[2], Christopher Aldo Rinaldi[3], Reza Razavi[1], Tobias Schaeffter[1], and Kawal S. Rhode[1]

[1] Division of Imaging Sciences and Biomedical Engineering, King's College London, SE1 7EH, UK
[2] Interventional X-ray, Philips Healthcare, Best, The Netherlands
[3] Department of Cardiology, Guy's & St. Thomas' Hospitals NHS Foundation Trust, London, SE1 7EH, UK
y.ma@kcl.ac.uk

**Abstract.** X-ray fluoroscopically-guided cardiac catheterization procedures are commonly carried out for the treatment of cardiac arrhythmias, such as atrial fibrillation (AF) and cardiac resynchronization therapy (CRT). X-ray images have poor soft tissue contrast and, for this reason, overlay of a 3D roadmap derived from pre-procedure volumetric image data can be used to add anatomical information. However, current overlay technologies have the limitation that 3D information is displayed on a 2D screen. Therefore, it is not possible for the cardiologist to appreciate the true positional relationship between anatomical/functional data and the position of the interventional devices. We prose a navigation methodology, called *cardiac unfold*, where an entire cardiac chamber is unfolded from 3D to 2D along with all relevant anatomical and functional information and coupled to real-time device tracking. This would allow more intuitive navigation since the entire 3D scene is displayed simultaneously on a 2D plot. A real-time unfold guidance platform for CRT was developed, where navigation is performed using the standard AHA 16-segment bull's-eye plot for the left ventricle (LV). The accuracy of the unfold navigation was assessed in 13 patient data sets by computing the registration errors of the LV pacing lead electrodes and was found to be 2.2 ± 0.9 mm. An unfold method was also developed for the left atrium (LA) using trimmed B-spline surfaces. The method was applied to 5 patient data sets and its utility was demonstrated for displaying information from delayed enhancement MRI of patients that had undergone radio-frequency ablation.

## 1 Introduction

Minimally-invasive catheter-based interventions have become the treatment of choice for patients with many forms of cardiovascular disease. The cardiac catheterization laboratory is the primary treatment environment for these procedures and X-ray fluoroscopy is the main imaging modality that is used for interventional guidance. Interventional devices, such as catheters, have been specifically designed to be

P. Abolmaesumi et al. (Eds.): IPCAI 2012, LNAI 7330, pp. 104–114, 2012.

highly-visible using fluoroscopy. However, navigation can be difficult because the target structures, such as the cardiac chambers and the great vessels, are not well-visualized using fluoroscopy without the use of repeated contrast agent injection. Long procedure times, high radiation dose and large contrast agent burden have lead to the introduction of image-guided navigation solutions. The use of this technology is exemplified in the case of electrophysiology (EP) procedures and cardiac resynchronization therapy (CRT). Examples of such technology include the EnSite Velocity (St. Jude Medical, USA), CARTO 3 (Biosense Webster, USA) and EP Navigator (Philips Healthcare, The Netherlands) systems. In each of these systems, three-dimensional (3D) anatomical models of the target cardiac chambers are used to guide the interventions. In the case of EnSite Velocity and CARTO 3, these models are reconstructed using tracked catheters that are moved inside the target chamber to generate the anatomy. In the case of EP Navigator, pre-procedural computer tomography [1], magnetic resonance imaging (MRI) [2], or rotational X-ray angiography [3, 4] of the heart are used to generate the anatomical models which are then registered to and overlaid onto X-ray fluoroscopy to provide a roadmap image.

Recently, the use of cardiac MRI to guide cardiac resynchronization therapy (CRT) for patients with heart failure has been proposed and demonstrated [5-7]. CRT involves the placement of a pacemaker device with pacing leads being inserted endocardially into the right atrium (RA) and right ventricle (RV), and epicardially into the left ventricle (LV) through the coronary venous system. There is potential to reduce the high failure rate (30%) of this procedure using advanced image-guidance. Cardiac MRI can be used to obtain all the critical information necessary for successful lead placement during CRT: (a) cardiac chamber anatomy; (b) coronary venous anatomy; (c) ventricular scar distribution; and (d) dyssynchrony information. Using a prototype version of the EP Navigator, we were previously able to place the LV pacing lead to target pre-selected segments of the LV based on the MRI information [5, 6].

One limitation of current navigation approaches is that the critical information required by the cardiologist for navigation is always displayed as a projection from 3D to 2D, i.e. on the computer display screen. In the case of anatomical overlay systems, such as EP Navigator, this means that the relationship between the position of interventional devices, such as the pacing leads, and the anatomical and functional information in the roadmap cannot easily be appreciated. In the case of electroanatomical mapping systems, such as EnSite Velocity or CARTO 3, there is frequent need to rotate the 3D anatomical models to obtain the correct view.

One way to overcome this limitation is to unfold the 3D information to 2D, something that has been applied extensively for the brain [8]. 2D representation of the LV using the American Heart Association (AHA) 16-segment bull's-eye plot is a well-established technique. Furthermore, it has been shown how additional information can be added to this. For example, Termeer *et al.* [9] presented combination of the coronary artery centreline and scar information on a bull's-eye plot. In this paper, this concept is extended for the use of interventional guidance by coupling the bull's-eye representation with real-time device tracking. A complete unfold guidance platform was developed for specific guidance of CRT procedures. Secondly, in order to extend the unfold concept for the guidance of radio-frequency ablation of atrial fibrillation, an unfold method for the left atrium (LA) surface was developed using trimmed B-spline surfaces. These unfolding techniques, termed

*cardiac unfold*, were applied to patient data: 13 data sets from patients undergoing CRT were used for off-line accuracy validation of the LV unfolding and real-time testing of the augmented navigation approach was used in 5 live CRT cases; for LA unfolding, only proof-of-concept is presented using 5 data sets from patients that underwent radiofrequency ablation for atrial fibrillation.

## 2 LV Unfolding Method

Cardiac MRI (Philips 1.5T Achieva, Phillips Healthcare, Best, The Netherlands) was performed prior to the pacemaker implants for 18 patients being treated for heart failure using CRT. Cardiac MRI consisted of a combination of anatomical and functional scans such as steady-state-free-precession (SSFP) and delayed enhancement (DE) scans. 3D SSFP whole-heart image data was automatically segmented to yield the endocardial surfaces of the RV, LA and RA and the endocardial and epicardial surfaces of the LV using a model-based segmentation algorithm [10]. The coronary veins and any myocardial scar were segmented from the MR images and dyssynchrony was quantified (see [6] for further details). Then the unfolding is carried out using the following methods:

### 2.1 3D to 2D Bull's-Eye Transformation

A transformation was designed to map the 3D anatomical/functional information to a 2D bull's-eye plot based on the standard AHA 16-segment model of the LV. An automatic method was designed using only the LV and RV surfaces which are extracted from the automatic segmentation results. A cubic Bezier curve is used to model the LV long axis. The cubic Bezier curve is defined as:

$$B(t) = (1-t)^3 P_0 + 3t(t-1)^2 P_1 + 3t^2(1-t)P_2 + t^3 P_3 \qquad t \in [0,1] \tag{1}$$

where $P_i$ are the control points. $P_0$ is the apex of the LV. $P_1$, $P_2$ and $P_3$ are the center points of cross sections perpendicular to the long axis. To search for the locations of the control points of the Bezier curve, the following 4 steps were used: Step (1): use the automatic whole-heart segmentation algorithm to segment the LV and RV from the whole-heart MRI data and extract the LV and RV surfaces using the marching cubes algorithm; Step (2): use a linear regression algorithm to calculate the principal axis of the LV surface (figure 1A). The principal axis is defined as the first eigenvector of the positive definite matrix $M_{pd}$, where $M_{pd} = (1/n)A^T A$. $n$ is the number of vertices in the LV surface. Matrix $A$ is defined as $A = V - \overline{V}$, where $V$ is the vertex array of the LV surface and $\overline{V}$ is the mean of all vertices; Step (3): project all vertices of the LV surface to the principle axis and find the lowest vertex. The lowest vertex is used as the apex of the LV; Step (4): calculate the center points of cross sections.

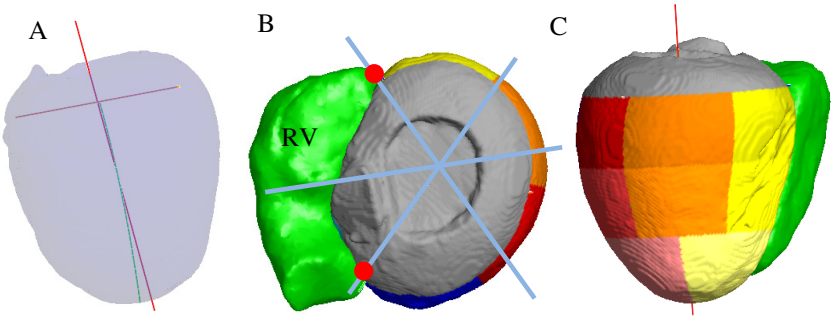


**Fig. 1.** (A) Principal axes (red lines) of the LV. The center Bezier curve (green curve). (B) Two landmarks (red spots) are used to divide the circular section into 6 segments. (C) Final result of automatic LV subdivision method.

After construction of the Bezier curve, it is used as the center curve of the LV surface (see figure 1A). The next step is to map all 3D vertices of the LV to the 2D bull's-eye plot. Similar to the standard LV subdivision method, two landmarks of each circular section are identified automatically by searching the attachment points of the RV to the LV (see figure 1B). This can be done in two steps: Step (1): calculate a line on the circular section from the center of the RV cross section to the center of the LV circular section; Step (2): use the line calculated in Step (1) as the reference line and search for the RV vertex in the RV cross section that forms the maximum angle between the reference line and the line from the RV vertex to the center of the LV circular section. Now, for any vertex on the LV surface, we can calculate its projection point on the center Bezier curve and obtain a parameter $t$ in the curve function $B(t)$. It can be used as the radius in the polar coordinate system (bull's-eye plot). The angle $\theta$ between the line from this vertex to the center of the circular section and the reference line can be used as the angle in the polar coordinate system. However, using the landmarks on the RV surface boundary will not always create 6 equal subdivisions of a full circle (each division should be $60°$ in the bull's-eye plot). Therefore, a linear warp function $W(\theta)$ is used to map the angle $\theta$ in the LV surface to the angle $W(\theta)$ used in the polar coordinate system. Finally, any 3D vertex $P(x, y, z)$ on the LV surface can be transformed into a 2D point $B(t, W(\theta))$ in the polar coordinate system. Figure 1C demonstrates the final result of our method.

## 2.2 Mapping 3D Coronary Sinus and Scar into 2D Bull's-Eye Plot

The coronary sinus (CS) is one of the key structures for CRT guidance. The 3D vertices on the CS model can be mapped into 2D by using the same transformation for mapping the LV surface. However, when mapping into 2D, the coronary vein triangulation topology will be lost. To re-triangulate the mapped 2D points, an unconstrained Delaunay triangulation was used (see figure 2A). Each triangle in the Delaunay triangulation is labeled as inside or outside based on the edge length rule

[11]. The edge length rule labels any triangle with any of its edges larger than a threshold as outside. The threshold is set to $\sqrt{3}$ times the voxel size in the 3D MR image. $\sqrt{3}$ was chosen based on the marching cubes algorithm, which states that the longest edge of a triangle is the diagonal of the voxel cube. After removing the outside triangles, the 2D model of the CS is generated (see figure 2B). Next, the binarized scar map, which represents the scar locations on the LV surface, is mapped into 2D. The 2D representation of scar is as a 2D mesh. Figure 2C gives an example of 2D representations of the CS and scar map.

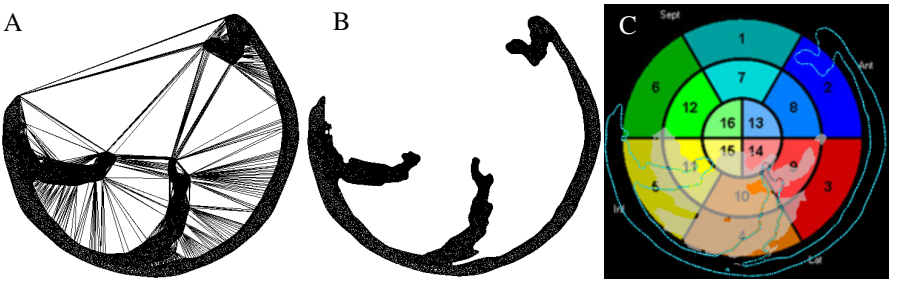


**Fig. 2.** (A) 2D Delaunay triangulation. (B) After removing the outside triangles. (C) The 2D bull's-eye plot with the CS (blue lines) and scar (transparent white mesh).

## 3 LA Unfolding Method

MR imaging was performed on 5 patients (mean age 60±10, 4 male) after radiofrequency ablation treatment for treatment of paroxysmal atrial fibrillation. This included Gadolinium-enhanced MR angiography (MRA) and DE imaging. The LA was automatically segmented from the MRA data using [12] followed by manual corrections by a clinical expert, when required. The LA surface was unfolded using the following steps:

### 3.1 Generation of B-Spline Contours

B-spline contours are obtained by scanning the LA segmentation in a raster-like fashion (see figure 3A) in the head-to-foot direction. Each scan line generates a contour. It is ensured that no multiple disjoint contours are generated for a single scan line. This can be a problem especially if the pulmonary veins (PVs) are not truncated at the ostium (see PV cut planes in figure 3A). Thus by carefully selecting appropriate cut planes to remove each pulmonary vein, each scan line only generates a single contour. For each contour, a distance-minimizing B-spline curve with 100 control points is then fitted through points sampled on the contour. B-spline curve fitting of these contours is important as it significantly reduces the noise within contour points.

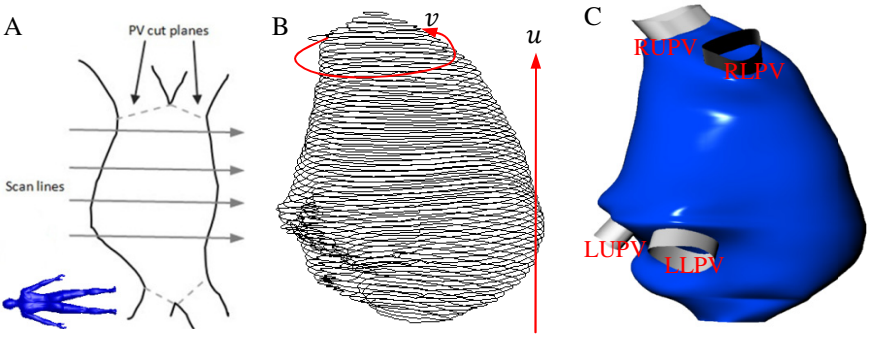


**Fig. 3.** (A) The generation of B-spline contours using scan lines. The human figure in the bottom-left indicates LA orientation. (B) B-spline curve contours. Arrows demonstrate the directions of $u$ and $v$ parameters. (C) B-spline surface constructed from the contours. Four cut-off PVs have been added for illustration purposes. (LUPV is left upper PV. LLPV is left lower PV. RUPV is right upper PV. RLPV is right lower PV).

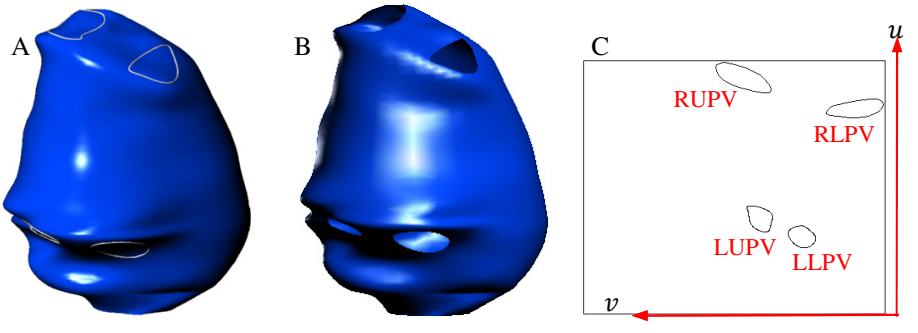


**Fig. 4.** (A) The LA surface with trimming curves. (B) The trimmed LA surface. (C) 2D *uv* map of the B-spline surface with 4 mapped trimmed curves.

### 3.2 Construction of B-Spline LA Model

A cubic B-spline surface is used to fit the main body of the LA from which 4 PVs have been cut and it is defined as $S(u,v) = \sum_{i=0}^{n}\sum_{j=0}^{m} N_{i,3}(u)N_{j,3}(v)P_{i,j}$. Where $\{P_{i,j}\}$ are the control points and $0 \le u,v \le 1$. $N_{i,3}(u)$ and $N_{j,3}(u)$ are cubic B-spline basis functions defined on the knot vector $U = \{u_0, u_1, \dots, u_{n+3+1}\}$ and $V = \{v_0, v_1, \dots, v_{m+3+1}\}$. The control point net $\{P_{i,j}\}$ is constructed from the control points of the B-spline curve contours. After the surface is constructed, it is rebuilt by undersampling the control points so that a smooth LA surface is created (see figure 3C). The rebuilt surface has 20x10 control points. Then 4 B-spline curves around the PV cutting regions are projected onto the B-spline surface to create 4 trimming curves (see figure 4A). The B-spline surface is trimmed in the region of the PVs using the trimming curves. The final result is shown in figure 4B.

### 3.3 Unfolding LA Surface into 2D Warped Parametric Map

The trimmed B-spline surface is first unfolded into the 2D parametric map (see figure 4C), which is generated after the trimmed surface is constructed. With the B-spline surface defined on $(u, v)$ parameters, the 3D surface is naturally unfolded into the 2D parametric map. The linearity between the 3D surface and the 2D parametric map needs to be improved, so that the surface distance on the LA between any pair of points is proportional to the distance between their mapped pairs on the 2D map. To achieve this, the 2D parametric map is warped along the directions of $u$ and $v$. As the LA B-spline surface is constructed from a series of evenly spaced 2D contours and $u$ is set as the direction along the contour level direction (see figure 3B), the distance traveled along the $u$ direction is linear. On the other hand, as contours at different levels have different lengths and the $v$ direction is set as the circular direction around the contours (see figure 3B), the distance traveled along the $v$ direction is non-linear. Therefore, the 2D parametric map needs to be warped along the $v$ direction to restore the linearity.

To warp the map, we first cut the trimmed B-spline surface at the iso-line ($v = 0.5$). The iso-line is defined by the points that have constant $u$ or $v$ values. The lengths of the iso-line segment ($0 \leq v \leq 0.5$) and the iso-line segment ($0.5 \leq v \leq 1.0$) at the evenly spaced $u$ levels (see figure 5A) are calculated and the 2D parametric map is warped along the $v$ direction according to the lengths of the iso-line segmentation (see figure 5B). In order to maintain the same length ratio between $u$ and $v$, the 2D parametric map is also scaled along the $u$ direction so that the length along the $u$ direction is equal to the length along the $v$ direction. The final result with the trimming curves is shown in figure 5C.

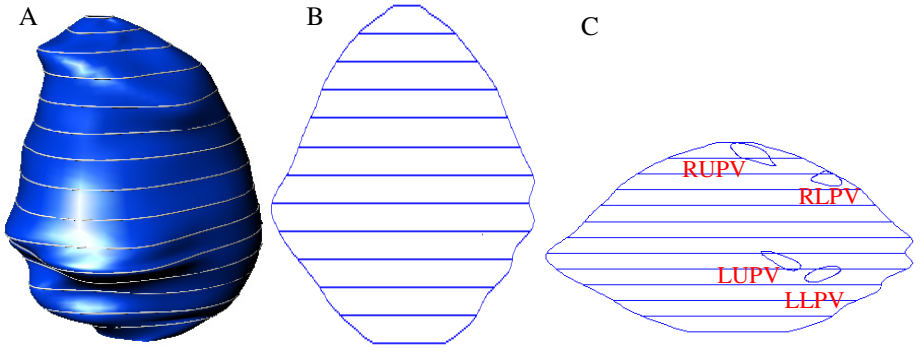


**Fig. 5.** (A) The iso-line segments at the evenly spaced $u$ levels. (B) The 2D parametric map warped along the $v$ direction. (C) The final result with trimming curves.

# 4 Results

## 4.1 The Accuracy of LV Unfolding Navigation

Unlike the LA surface unfolding, the LV surface unfolding method directly uses the LV mesh and transfers to 2D polar coordinates. Therefore, there are no model or surface fitting errors. Instead, we investigated the navigation accuracy using the LV unfolding method. 13 datasets from 13 patients were used for off-line validation. The MR data was of sufficient quality to allow the generation of the coronary venous system including the main three sub-branches. The models were registered successfully to the X-ray fluoroscopic data in all cases. The details of the registration method can be found in [6]. The respiratory motion was compensated by tracking the diaphragm in the X-ray images [13]. The registration errors in the 2D bull's-eye plot were calculated as the mean distance between the 2D pacing lead electrode positions (see crosses in figure 6) and the center curve of the CS sub-branches. The mapped lead position is automatically calculated and the centreline is manually defined. The measured error is the total error in the navigation system and encompasses all steps from segmentation to unfolding and registration to device tracking. An accuracy of $2.2 \pm 0.9$ mm was achieved for 602 X-ray fluoroscopic images from the 13 cases. The pixel to mm transformation was achieved by using the radius of the bull's-eye plot. In the 3D anatomical model derived from MR data, the radius corresponds to the distance from the apex to the center of the mitral valve along the long axis of the LV. Therefore, a ratio between the pixel size in the 2D bull's-eye plot and mm in the 3D anatomical model can be calculated.

For the real-time testing of the unfold guidance in 5 clinical cases, the 2D bull's-eye guidance platform was able to record and display different LV lead pacing positions both in the 3D overlay view and in the 2D bull's-eye view together with the dyssynchrony color map. The clinician was able to successfully place the pacing lead in the targeted LV segment with adequate pacing thresholds.

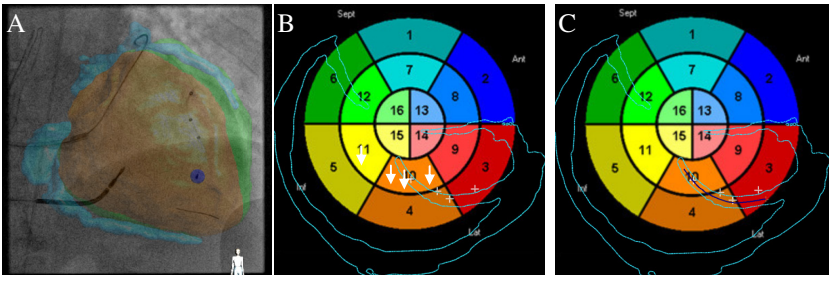


**Fig. 6.** (A) Overlay of the LV and CS onto an X-ray image. The blue sphere is the position of the lead electrode. (B) 2D unfolding navigation screenshot. The light blue contour is the CS tree unfolded in the 2D bull's-eye plot. The white crosses are the positions of the pacing leads. (C) Screenshot with the manual annotation of the centerline of the CS sub-branch (the dark blue line).

### 4.2 LA Unfolding Accuracy

To test the accuracy of the LA surface unfolding, 5 patient datasets were used (patient mean age 60 ± 10, 4 male and 1 female). Since we have only reached the unfolding stage for the LA, the only measure of error that we can currently quote is the surface fitting error as the initial B-spline surface fitting is an approximation. The surface fitting error is the Euclidean distance error between the vertices on the LA mesh which is directly extracted from the LA segmentation result (after removing 4 PVs) and projected points on the B-spline surface. An overall error of 0.8 ± 0.8 mm was achieved for the 5 data sets. Figure 7A gives the error color map on the fitted B-spline LA surface. To demonstrate potential use of the LA unfolding method, a lesion map created from the delayed enhancement MRI was used to generate a 2D unfolding color map [14]. This could be used together with MRI-derived LA model guidance to redo ablation procedures as it gives information about previously ablated areas (red regions in figure 7B and 7C).

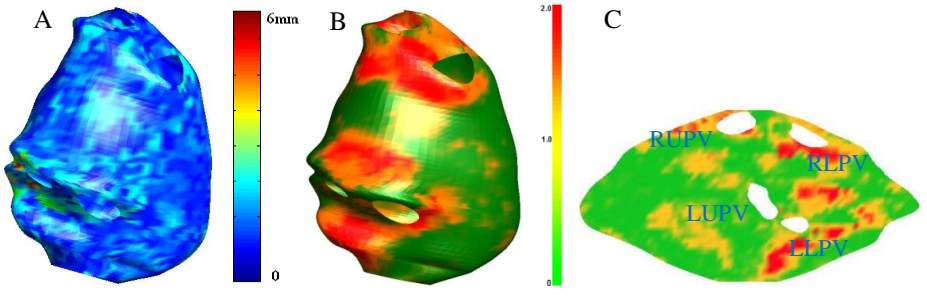


**Fig. 7.** (A) Color map for surface fitting errors. (B) 3D lesion map created from the delayed enhancement MRI. (Scale for the color bar is the number of standard deviations from the mean of blood pool intensity.) (C) 2D unfolding lesion map.

## 5 Discussion and Conclusion

This paper describes the implementation of *cardiac unfold* in CRT procedures (LV unfolding) and atrial fibrillation ablation procedures (LA unfolding). The 2D bull's-eye guidance platform for CRT procedures allows simultaneous visualization of the LV and coronary vein morphology, myocardial scar distribution, dyssynchrony information and pacing lead position for the entire LV in real-time. The methodology was validated using 13 data sets from patients that underwent CRT and the accuracy of mapping the pacing lead position to the bull's-eye plot was calculated to be approximately 2 mm, which is well within the requirements of clinical accuracy. The guidance platform was tested on 5 live cases and proved successful to allow navigation for LV lead implantation. Furthermore, the technique of LA surface unfolding was also demonstrated in this paper. The average unfolding error was less than 1 mm in 5 patient data sets. This technique could be useful for navigation since it allows the visualisation of large amounts of complex geometric and functional

information in a single 2D representation. It could also be useful if coupled to a robotic catheter system to reduce the degrees of freedom in the control interface.

In conclusion, *cardiac unfold* techniques are promising for augmenting image-based navigation for catheter-based cardiac interventions. Further, validation and testing of these will be required to prove clinical utility.

## References


1. Sra, J., Narayan, G., Krum, D., Malloy, A., Cooley, R., Bhatia, A., Dhala, A., Blanck, Z., Nangia, V., Akhtar, M.: Computed tomography-fluoroscopy image integration-guided catheter ablation of atrial fibrillation. Journal of Cardiovascular Electrophysiology 18(4), 409–414 (2007)
2. Rhode, K.S., Hill, D.L.G., Edwards, P.J., Hipwell, J., Rueckert, D., Sanchez-Ortiz, G., Hegde, S., Rahunathan, V., Razavi, R.: Registration and tracking to integrate X-ray and MR images in an XMR facility. IEEE Transactions on Medical Imaging 24(11), 810–815 (2003)
3. Pruemmer, M., Hornegger, J., Lauritsch, G., Wigstrom, L., Girard-Hughes, E., Fahrig, R.: Cardiac C-arm CT: a unified framework for motion estimation and dynamic CT. IEEE Transactions on Medical Imaging 28(11), 1836–1849 (2009)
4. Orlov, M.V., Hoffmeister, P., Chaudhry, G.M., Almasry, I., Gijsbers, G.H., Swack, T., Haffajee, C.I.: Three-dimensional rotational angiography of the left atrium and esophagus–A virtual computed tomography scan in the electrophysiology lab. Heart Rhythm 4(1), 37–43 (2007)
5. Duckett, S.G., Ginks, M.R., et al.: Advanced image fusion to overlay coronary sinus anatomy with real time fluoroscopy to facilitate left ventricular lead implantation in CRT. Pacing Clin. Electrophysiol. 34(2), 226–234 (2010)
6. Ma, Y., Duckett, S., Chinchapatnam, P., Shetty, A., Aldo Rinaldi, C., Schaeffter, T., Rhode, K.S.: Image and Physiological Data Fusion for Guidance and Modelling of Cardiac Resynchronization Therapy Procedures. In: Camara, O., Pop, M., Rhode, K., Sermesant, M., Smith, N., Young, A. (eds.) STACOM 2010. LNCS, vol. 6364, pp. 105–113. Springer, Heidelberg (2010)
7. Manzke, R., Bornstedt, A., et al.: Respiratory motion compensated overlay of surface models from cardiac MR on interventional x-ray fluoroscopy for guidance of cardiac resynchronization therapy procedures. In: SPIE Medical Imaging 2010: Visualization, Image-Guided Procedures, and Modeling, vol. 7625 (2010)
8. Drury, H.A., Van Essen, D.C., et al.: Computerized mappings of the cerebral cortex: a multiresolution flattening method and a surface-based coordinate system. J. Cogn. Neurosci. 8, 1–28 (1996)
9. Termeer, M., Bescós, J.O., Breeuwer, M., Vilanova, A., Gerritsen, F.A., Gröller, M.E., Nagel, E.: Visualization of myocardial perfusion derived from coronary anatomy. IEEE Trans. Vis. Comput. Graph. 14(6), 1595–1602 (2008)
10. Peters, J., Ecabert, O., Meyer, C., Schramm, H., Kneser, R., Groth, A., Weese, J.: Automatic Whole Heart Segmentation in Static Magnetic Resonance Image Volumes. In: Ayache, N., Ourselin, S., Maeder, A. (eds.) MICCAI 2007, Part II. LNCS, vol. 4792, pp. 402–410. Springer, Heidelberg (2007)
11. Ma, Y., Saetzler, K.: A parallelized surface extraction algorithm for large binary image data sets based on adaptive 3-D Delaunay subdivision strategy. IEEE Transactions on Visualization and Computer Graphics 14(1), 160–172 (2008)

12. Karim, R., Mohiaddin, R., Drivas, P., Rueckert, D.: Automatic extraction of the left atrial anatomy from MR for atrial fibrillation ablation. In: Proceedings of IEEE International Symposium on Biomedical Imaging (2009)
13. Ma, Y., King, A., Gogin, N., Gijsbers, G., Rinaldi, C.A., Gill, J., Razavi, R., Rhode, K.: Clinical evaluation of respiratory motion compensation for anatomical roadmap guided cardiac electrophysiology procedures. IEEE Transactions on Biomedical Engineering 59(1), 122–131 (2011)
14. Knowles, B., Caulfield, D., et al.: Three-dimensional visualization of acute radiofrequency ablation lesions using MRI for the simultaneous determination of the patterns of necrosis and edema. IEEE Trans. Biomedical Engineering 57(6), 1467–1475 (2010)